Nuclear Instruments and Methods in Physics Research B 547 (2024) 165213

Contents lists available at ScienceDirect

Nuclear Inst. and Methods in Physics Research, B

journal homepage: www.elsevier.com/locate/nimb

Characterization of the field ionization extension for the laser ion source and trap: Measurement of the ionization potential of ytterbium

Magdalena Kaja [a,*], Dominik Studer [b,c], Reinhard Heinke [d], Tom Kieck [b,c], Klaus Wendt [a]

[a] Institute of Physics, Johannes Gutenberg University Mainz, Germany
[b] GSI Helmholtzzentrum für Schwerionenforschung GmbH, Darmstadt, Germany
[c] Helmholtz Institute Mainz, Germany
[d] STI group, SY Department, CERN, Switzerland

ARTICLE INFO

Keywords:
Resonance ionization laser ion source
Laser spectroscopy
Electric field ionization

ABSTRACT

We report on the development and application of the Field Ionization Laser Ion Source and Trap (FI-LIST) at the RISIKO mass separator at Mainz University. The FI-LIST is an adaptation of the well-established LIST unit developed at Mainz and successfully adapted to CERN-ISOLDE. It is specifically designed for field ionization of highly excited atoms in a homogeneous electric field. To assess the performance of the device for future use on radioactive species of e.g. actinides, we conducted ionization potential (IP) measurements on ytterbium, for which the IP is precisely known. The IP value was derived by applying the saddle-point model with a relative precision of $3 \cdot 10^{-6}$ and in very good agreement with the literature value.

1. Introduction

The ionization potential (IP) is a fundamental property of each individual chemical element, representing the energy required to remove an electron from the neutral atom. However, IP values for more than 20 elements of the Periodic Table are found in literature only with rather large uncertainty above 1 cm^{-1}, corresponding to a relative precision of 10^{-5} and above, which excludes the use of these values for any valuable atomic or molecular estimations [1]. This limitation is particularly pronounced for elements that have no stable isotopes or those produced only artificially. A common method of determining the IP with precision in the order of 0.1 cm^{-1} or better is the analysis of Rydberg series converging to the IP. Lately, this approach was successfully employed to determine the IP of various radioactive elements such as Tc [2], Po [3,4], At [5], or different members of the actinide series, i.e. Ac [6], Cm [7], Es [8] or No [9]. However, with such complex atomic spectra as particularly found in the lanthanide and actinide series featuring an open f shell, unambiguous identification of individual members of a specific Rydberg series becomes exceedingly difficult. The presence of numerous resonances accentuated by influences arising from strong configuration mixing makes it challenging or sometimes even impossible, to identify or assign levels properly. A prime example illustrating this situation is found in the element Pa with Z = 91, which even exhibits chaotic behavior strongly affecting level positions and densities almost along the entire energy range between the ground state and the IP [10,11].

These restrictions, specifically but not exclusively found in f-element spectra, call for an alternative method to precisely determine the IP apart from studying Rydberg convergences. In this work, we present the approach that involves the ionization of highly excited atoms in a well-controlled static electric field, which is provided within a newly developed laser ion source unit for direct application at off-line and on-line mass separator facilities. A similar technique was already used more than 25 years ago by Köhler et al. [12] and Erdmann et al. [13] for measurements of IPs of numerous actinide elements at a time-of-flight (TOF) mass spectrometer. These pioneering studies provided a precision in the IP determination of about 2 cm^{-1}, which has not yet been surpassed for 6 out of the initially studied 10 actinides [1]. More recently, this technique was adopted for IP determination in the radioactive lanthanide element Pm by Studer et al. [14] and in the actinide Cm by Kneip et al. [7] in our laboratory. In both cases, the control of the ionizing electric field was facilitated by using a quadrupole mass spectrometer with moderate ion acceleration, while transmission and sensitivity were limited and sample sizes in the order or well above 10^{13} atoms had to be used.

To enhance the sensitivity and efficiency of this technique, allowing access to elements that are only available in small sample sizes, as e.g., heavy actinides or on-line produced short-lived radioactive isotopes, the device FI-LIST was constructed. It is a further generation of the Laser Ion Source and Trap (LIST) developed initially at Mainz

* Corresponding author.
E-mail address: mkaja@uni-mainz.de (M. Kaja).

https://doi.org/10.1016/j.nimb.2023.165213
Received 12 October 2023; Received in revised form 21 November 2023; Accepted 15 December 2023
Available online 22 December 2023

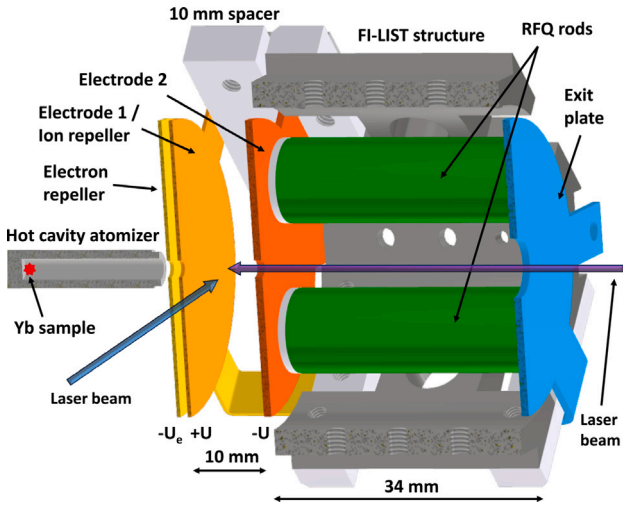

Fig. 1. Technical drawing with half-cut of the Field Ionization Laser Ion Source FI-LIST. The electron repeller is located directly ~1 mm behind the hot cavity atomizer. Ionization occurs at the center region, between electrode 1 and electrode 2, where both lasers and the effusing atom beam intersect. Additionally, electrode 1 acts as an ion repeller having a positive voltage. All front electrodes have a 2 mm diameter orifice to minimize the fringe perturbation of the electric field.

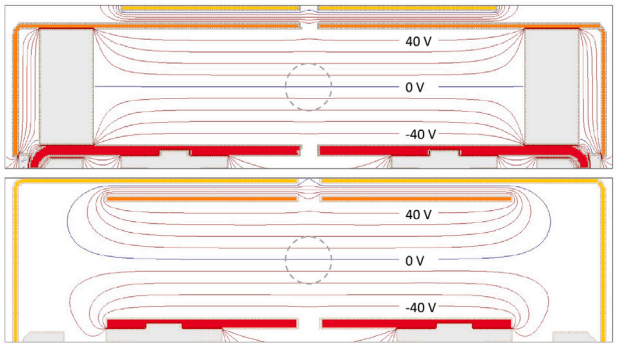

Fig. 2. Simulation showing the potential lines between the FI-LIST front electrodes for the electric field of 100 V/cm in both transversal directions. The lines are drawn from 40 to −40 V in steps of 10 V with the central blue line indicating 0 V. Cuts are made in a way to include the influences of the electrode mountings. The interaction area with a radius of 2 mm is indicated by the central circle. The SIMION 8.1 drawing is recolored to match the colors in Fig. 1.

University [15–17] and afterwards implemented successfully at CERN-ISOLDE for high-selectivity measurements on exotic species [18,19]. High-purity ion beams are provided by this type of source thanks to the particularly efficient reduction of background by suppression of surface ionized species. Additionally, a specific version for high-resolution laser spectroscopy on optical hyperfine structures and isotope shifts was developed as PI-LIST (Perpendicularly Illuminated LIST) ion source. It implements a perpendicular intersection of the thermal atomic beam from the atomizer furnace and the first step excitation laser for reduction of Doppler broadening in a crossed laser beam — atom beam geometry [20,21]. LISTs, in all their variations, are ion-source modules that can be easily integrated into various setups and apparatus.

To demonstrate the performance and precision of the newly designed FI-LIST ion source unit, laser spectroscopy of ytterbium was conducted at the RISIKO mass separator at Mainz University [22] with the goal of determining the IP through field ionization using the saddle point model (see Section 4). Ytterbium with Z = 70 and being the second-to-last element in the lanthanide series, has a ground state configuration of [Xe] $4f^{14}6s^2\ {}^1S_0$. The 4f shell is fully occupied with 14 electrons and thus the ground state is very pure (>99%) with only negligible admixtures from e.g. the 5d shell [1]. Correspondingly, a very clear two-electron alkaline-earth-like spectrum is resulting. This feature allowed the analysis of the 6sns and 6snd Rydberg series up to principal quantum numbers of n = 80 using laser-microwave double resonance spectroscopy [23]. The authors performed a careful analysis of these data using a multichannel-quantum-defect-theory (MQDT) approach that led to an exceptionally precise value of the IP of $50443.07041(25)\,\mathrm{cm}^{-1}$ for the isotope ^{174}Yb. This highest precision IP value beyond Cs (Z = 55) makes ytterbium an ideal candidate for benchmarking the FI-LIST ion source and evaluating the achievable precision for IP determination in any other element in the heavy mass regions of lanthanides and actinides.

2. FI-LIST design and implementation

The central component of the FI-LIST is based on aspects of the rather similar designs of the LIST and the PI-LIST. Both use a linear radiofrequency quadrupole (RFQ) structure with rods of 10 mm diameter and a free field radius of 7.5 mm, operating with a radiofrequency voltage with about 1.2 MHz frequency and an amplitude of up to $V_{rf} \sim 500\ V_{pp}$ to provide transversal guidance of ions towards the acceleration stage of the subsequent mass separator. In contrast to the length of 90 mm for the LIST and PI-LIST units, as operated at CERN, a much shorter length of only 34 mm has been used in the FI-LIST to give space for the location of the laser-atom interaction region just between the hot cavity atomizer and the RFQ structure. A further difference is the design of this interaction region. The FI-LIST is equipped with three electrodes in front of the RFQ structure acting as an electron repeller, an ion repeller (called electrode 1), and an additional electrode 2 (see Fig. 1). The electron repeller is placed ~1 mm behind the hot cavity atomizer, followed immediately by the ion repeller 0.5 mm behind it. These two electrodes allow suppression of electrons, which may cause electron impact ionization in the LIST volume, and non-laser ionized species emitted from the hot cavity by surface ionization or collisions. The laser excitation and field ionization process takes place in the central spot of the region between electrode 1 and electrode 2, which are separated by a precisely fixed distance of 10.00 ± 0.05 mm. To define and maintain this distance, which determines the field strength, two corresponding insulating ceramic spacers are installed at the mount of the electrodes. The presence of a uniform electric field is crucial in the central interaction region between electrodes 1 and 2. Its exact value and orientation might be affected by field leakages through the two central bores in the electrodes, which are necessary for the entrance of the atoms and the exit of the ions. Simulations using the SIMION 8.1 code [24] demonstrated that the condition of a suitable uniform field is met for holes with a diameter of 2 mm. An example of the simulation of an electric field of 100 V/cm is depicted in Fig. 2. In the central interaction region with a laser spot size of < 4 mm diameter including possible slight misalignment of the lasers, a field is not perfectly homogeneous which is taken into account in the error analysis. Within that region, for all electric fields within the range of 200 V/cm down to 5 V/cm, the simulated value has a deviation of less than −1% to the nominally applied one. The deviation becomes more significant below 5 V/cm to the observed maximum of −5% at 1.02 V/cm. The accurate potential difference between electrodes 1 and 2 was measured with a multimeter (Keithley 2700) with a precision of about 10^{-4}. For analysis, the field values were extracted from the simulations with the input of the measured potential difference.

After successful resonant laser excitation of the atoms in the interaction spot and subsequent field ionization, the ions are pulled towards electrode 2 and continue their trajectory through the guiding RFQ structure, which in addition serves as a shield against any disturbing influences of the high acceleration voltage of the mass separator. To maintain a stable value of the total acceleration potential at the interaction spot and prevent undesired behavior within the RFQ structure,

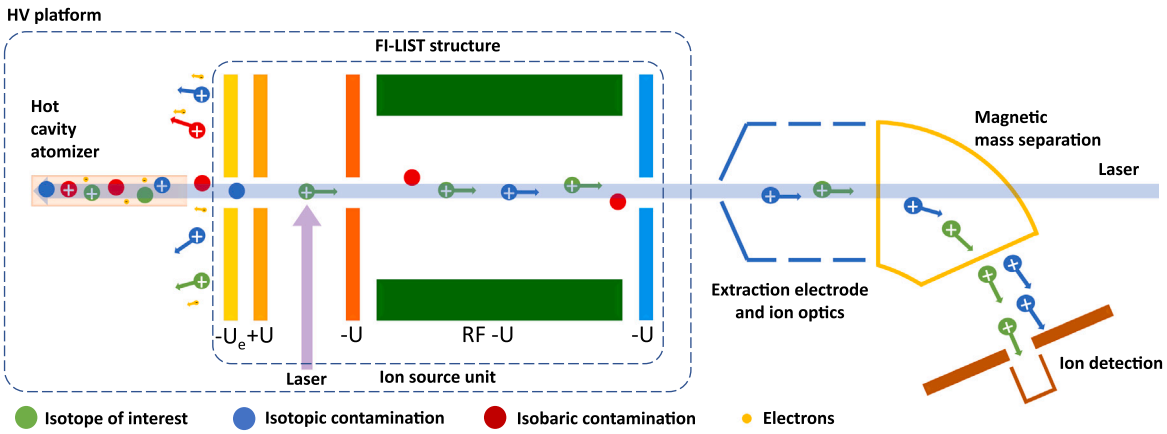

Fig. 3. Schematic sketch of the FI-LIST installed at the RISIKO mass separator. Ionization occurs at the central spot between electrodes 1 (orange) and 2 (red), where the perpendicular laser beams intersect with the atomic and a possible anti-collinear laser beam. The created ions are subsequently guided by the RFQ structure towards the mass separator. After extraction, acceleration, and ion optical beam shaping, the ions undergo mass selection in the sector field magnet and are quantitatively counted by a MagneTOF detector.

electrode 1 is set on the opposite voltage (+U) of electrode 2 (-U), which is also applied as a DC offset of the RFQ rods as well as to the exit electrode. Just during electric field scans one of the two electrodes is scanned in the near vicinity of the absolute value of the other.

As shown in Fig. 3, the entire FI-LIST unit is placed on the high voltage platform of the RISIKO mass separator at a potential of 30 kV. The ytterbium sample material is placed inside the 35 mm long tantalum tube atomizer of 2.5 mm inner diameter, which is resistively heated to about 700 to 1000 °C for atomization of Yb. The atomizer can be operated up to a maximum temperature of 2000 °C necessary e.g. for efficient evaporation of actinides and refractive metals. After ionization inside the FI-LIST, acceleration, and mass separation the ions are detected by a single ion counting detector (MagneTOF™, ETP electron multipliers).

A two-step resonance excitation process is induced by using the light of two tunable Ti:sapphire lasers pumped by 15 W each of a commercial frequency-doubled Nd:YAG laser at 532 nm with a 10 kHz repetition rate (Photonics Industries DM100-532). For the first transition, a so-called standard Ti:sapphire of the Mainz University design is used with a typical pulse length of 50 ns, a spectral linewidth of 5 GHz, and up to 4 W average output power [25]. For the second step, a grating-tuned Ti:sapphire laser is employed allowing mode-hope-free tuning in the entire spectral range covered with an output power of up to 2 W and a spectral linewidth of 2–5 GHz [26]. Each of these lasers has a tuning range of 700–1000 nm, which can be extended to the range of 350–490 nm by second harmonic generation using a resonator-internal frequency doubling process within a beta barium borate (BBO) crystal. The fundamental frequency of each laser was measured by a commercial wavemeter (High Finesse WS6-600), with an accuracy not better than 20% of the laser linewidth. There are different arrangements to send laser beams into the FI-LIST. Both lasers can be introduced perpendicular to the FI-LIST axis, or one of the lasers can be arranged to enter anti-collinearly to the ion beam. For the measurements discussed here, we exclusively used perpendicular irradiation for both laser beams with respect to the atomic beam axis.

3. Laser spectroscopy on Yb

Ytterbium atoms were excited from the atomic ground state $4f^{14}6s^2\ ^1S_0$ to Rydberg states of even parity using a two-step excitation scheme along the intermediate level $4f^{14}6s6p\ ^1P_1^o$ at 25068.22 cm^{-1}, which is pure to about 73% [1]. The second step was scanned using the grating laser in the range of 25259 cm^{-1} to 25322 cm^{-1}. The relative polarizations of the laser are known to play a significant role in the

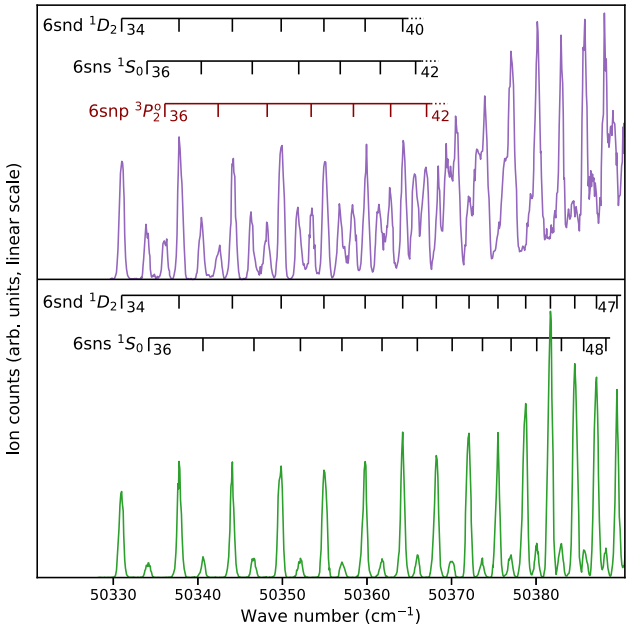

Fig. 4. Second step laser scans at electric fields of 20 V/cm (upper trace) and 0 V/cm (lower trace), respectively. Each Rydberg series is indicated by a comb above the spectra. More details are provided in the text.

efficiency of a multi-step excitation process into different Rydberg series due to the selection rules of individual magnetic sublevels. This effect has been studied in great detail by Li et al. in Be [27] and is similarly relevant here, as the spectrum of Yb is isoelectronic to Be and also the ground state has J = 0. We have experimentally tested this influence and optimized the spectroscopic arrangement accordingly. As a consequence of these qualitative tests and in accordance with the findings of [27], parallel polarization of both lasers was used throughout our studies. Fig. 4 shows laser scans for the ionization step within the field strength of 20 V/cm (upper traces) in comparison to the field-free case (lower traces). In both cases, the ionization occurs through unselective processes, which are rather inefficient, and a significantly higher atomizer temperature was required. In the lower spectrum, the resonances originate from strong transitions into the members with n = 34 to n = 48 of the $4f^{14}6snd\ ^1D_2$ Rydberg state series, and significantly weaker into the members n = 36 to n = 49 of the $4f^{14}6sns\ ^1S_0$ series. All

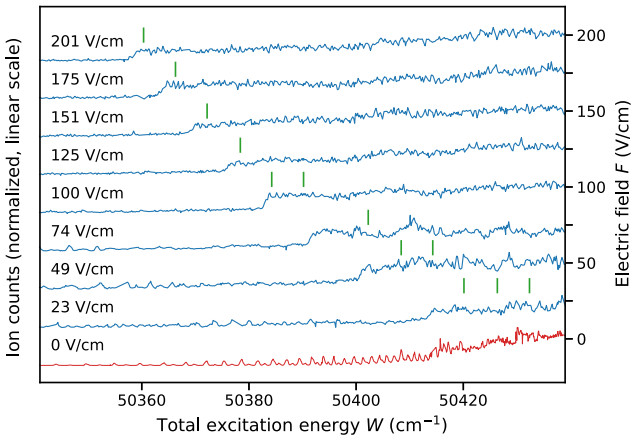

Fig. 5. Scans of the second step laser under different conditions. The blue scans represent the laser scans conducted at various electric fields F_i with the corresponding electric field value indicated. The 12 green lines denote the total energy values of the laser excitation for which individual field scans were carried out. The lowest red trace represents a laser scan performed at 0 V/cm, where ionization takes place through unselective processes. For more details see text.

resonances are well resolved and no significant background is observed due to the relatively low operation temperature of the atomizer cavity. All total excitation energy positions are in good agreement with the much more extensive and precise data of [23]. In the case of the external field of 20 V/cm, we observe a significant change in the intensity ratio of the two series mentioned as well as one additional series which can be assigned to $4f^{14}6s(^2S_{1/2})np\ ^3P_2^o$ [28]. While transitions into this series from the chosen first excited state are forbidden due to no parity change, in the presence of the electric field, the mixing of states and the violation of parity selection occurs due to the Stark effect. This was similarly seen by Li et al. [27] even for weak unshielded stray fields. Another consequence is the incremental shifting, broadening, and splitting of the Rydberg peaks within the electric field, which is observed with a rather sharp onset at energies above 50360 cm^{-1} accompanied by a gradually increasing baseline beyond this energy. Additionally, closer to the IP, individual Rydberg peaks are no longer resolved in the external field, but the ionization continuum is shifted towards lower energies as a function of the strength of the applied electric field. This effect is visualized in Fig. 5 and has been used for IP determination from the ionization threshold as discussed below.

4. Ionization potential

For testing and characterizing the FI-LIST regarding its accuracy for the determination of unknown ionization potentials, an IP value for Yb was determined from the excitation into highly excited states within different external electric fields. The saddle point model, as extensively discussed by Littman et al. [29] was used for theoretical description. The threshold W_s at which ionization occurs is therein given by

$$W_s = \mathrm{IP} - 2\sqrt{\frac{Z_{\mathrm{eff}} e^3 F}{4\pi\epsilon_0}}. \tag{1}$$

Here, Z_{eff} represents the effective charge of the atomic core, and F is the strength of the external field. For highly excited states, we can simplify Eq. (1) by assuming $Z_{eff} = 1$, resulting in $W_s = \mathrm{IP} - 6.12(\mathrm{Vcm})^{-1/2} \cdot \sqrt{F}$. Thus, by precisely measuring several field ionization thresholds W_s and extrapolating to zero-field strength, we can determine the IP.

Corresponding scans of the second step laser below the IP were performed for different electric fields. The results are depicted in Fig. 5. As expected, the threshold is progressively shifted towards lower energies for increasing electric field strengths according to Eq. (1). Individual Rydberg peaks, as observed in the lowest plot representing the spectrum without any electric field contribution, are no longer present. The plot indicates a somewhat different behavior from observations in Pm [14], where peaks were still observed in the presence of electric field. These seemingly were not Rydberg states, which would have been strongly affected by the electric field due to their high polarizability.

The occurrence of the onset of the ionization within rather unstructured spectra led us to two alternative approaches for determining the IP: (a) scanning the wave number of the second step laser for a series of electric field strengths, or alternatively (b) scanning the electric field within the expected threshold range for different fixed wavelengths of the second excitation step, which are marked as green dashes in Fig. 5. Both measurements were carried out by scanning the corresponding parameter, i.e. laser frequencies or, alternatively, electric potentials, both in upward and downward direction to prevent any hysteresis-like influences from a possibly slightly delayed data acquisition. Approach (a) involved measuring 14 different thresholds by scanning the second step laser for about 25 cm^{-1} resulting in a total of 28 separate measurements. Approach (b) focused on investigating 12 thresholds by scanning the field strengths by accordingly controlling either electrode 1 or electrode 2, resulting in a total of 24 scans. One typical example of a scan within approaches (a) and (b), respectively, is shown in Fig. 6. The data, which in both cases represents a convolution of a step function of the onset of ionization at the threshold with the Gaussian function of the laser frequency distribution, is described well by a sigmoid function

$$S(X) = A_0 + \frac{A_1}{1 + e^{-k(X - X_T)}}, \tag{2}$$

with an offset A_0, amplitude A_1, exponential coefficient k determining the width, and turning point X_T. The latter was taken as the ionization threshold for the corresponding electric field or alternatively the respective wave number (depending on the approach), following the approach as discussed in great detail in [14]. As can be seen in Fig. 5, all step functions at fixed field strength have a spectral width in the order of 0.5 to 1 cm^{-1}, which roughly matches the laser linewidth. This justifies the identification of the turning point as the ionization threshold, which is confirmed by the very good agreement of the data obtained for the field scans at fixed laser frequency.

The obtained thresholds are denoted as W_s^λ for wavelength scans with fixed F and W_s^F for scans of field strength at fixed wavelengths, respectively. Electric field strengths were determined from the differences of the measured potentials at electrodes 1 and 2 and the error includes the field deviations estimated by SIMION as discussed in Section 2. To determine the IP, the obtained data of the fitted W_s from both approaches were plotted as a function of $\sqrt{F}$ in Fig. 7. The blue and orange colors of data points correspond to approaches (a) and (b), respectively. In both cases, the data exhibit a perfectly linear trend that can be fitted using Eq. (1). That yields

$$W_s^\lambda = 50443.05(15)\,\mathrm{cm}^{-1} - 6.034(10)\{30\}\,(\mathrm{Vcm})^{-1/2} \cdot \sqrt{F}, \tag{3}$$

$$W_s^F = 50443.21(13)\,\mathrm{cm}^{-1} - 6.050(7)\{30\}\,(\mathrm{Vcm})^{-1/2} \cdot \sqrt{F}, \tag{4}$$

where round brackets indicate statistical error, and curly brackets indicate systematic error. These values indicate an IP of $50443.05(15)\,\mathrm{cm}^{-1}$ and $50443.21(13)\,\mathrm{cm}^{-1}$, respectively, demonstrating very good agreement, both between the two approaches and with the literature value of 50443.07041(25) cm^{-1} [23]. Consistency is also found for the line slopes, which, however, are slightly smaller than the value of 6.12 $(\mathrm{Vcm})^{-1/2}$ predicted by the saddle point model. That behavior was also seen by Merkt et al. [30], Studer et al. [14], and Kneip et al. [7]. As discussed in detail in the literature, e.g. in [14,30], this observed discrepancy can be attributed either to a slight deviation in the distance between the electrodes or alternatively to contributions by the Stark effect, which are ignored in the simple saddle point model. Under all circumstances, the distance between the electrodes affects only the slope of the line and does not alter the intersection of the line with the y-axis, i.e. the IP, which for that reason only shows a statistical

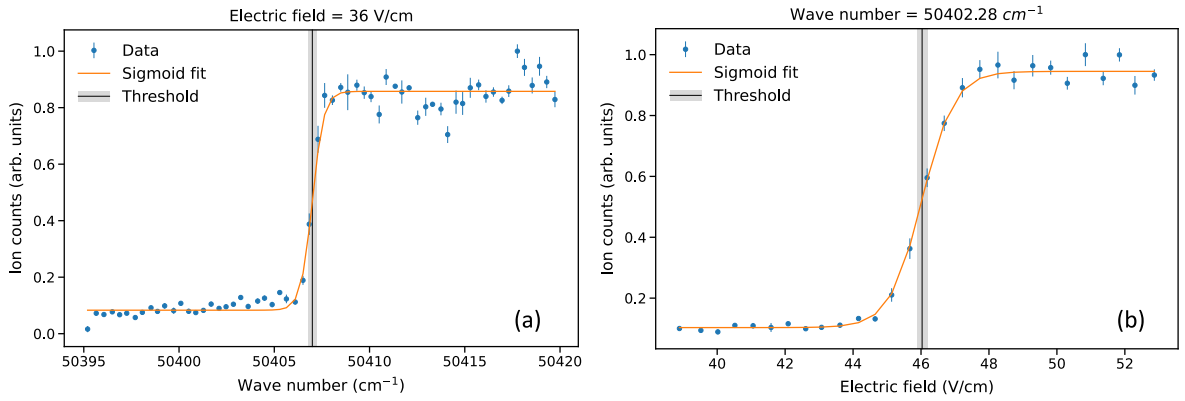

Fig. 6. The examples of (a) a laser scan at a fixed voltage of 36 V/cm according to approach (a), and (b) an electric field scan at a fixed laser wave number of 50402.28 cm^{-1} according to approach (b). In both cases, the ionization threshold corresponds to the turning point of the sigmoid fit. The gray shaded area indicates the uncertainty.

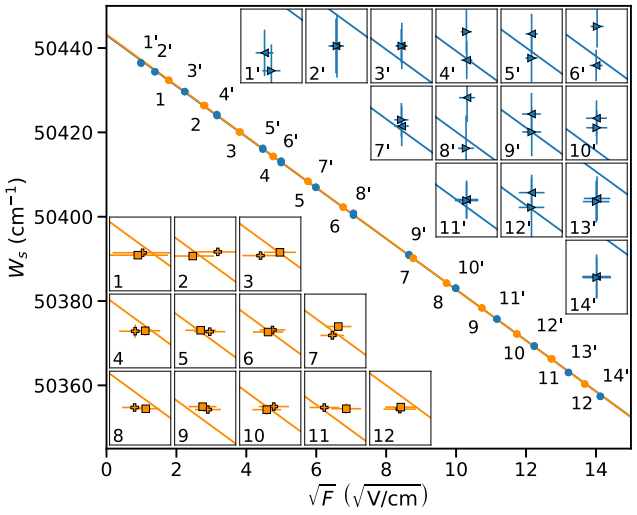

Fig. 7. Extracted ionization thresholds of the two approaches given as a function of the square root of the electric field strength. The orange data points indicate the thresholds of the field scans and the inset indicates which electrode was scanned — electrode 1 is represented by plus and electrode 2 by a square. The blue data points represent the thresholds of the wavelength scans and the arrows in the inset represent the direction of the scanning (e.g. left pointing arrow means the downward scanning). The orange and blue lines correspond to the fitted curves for the respective data sets. The insets display an enlarged view of the deviation between the data points and the fitted line, with a magnification factor of 25.

error. By considering a minor change of the electrode distance of about +0.1 mm, which might have occurred during installation, the line slope would perfectly reproduce the expected value.

5. Conclusion and outlook

The FI-LIST ion source unit, which was specifically designed for field ionization within a well-controlled electric field, was employed and was characterized at the RISIKO mass separator on IP measurements in ytterbium, which exhibits a clear and well-known Rydberg spectrum below the IP. Two different approaches to determine the IP were compared. Regardless of whether field-dependent ionization thresholds were obtained by fixing the electric field and scanning the laser wave number or alternatively by fixing the laser wave number and scanning the electric field, the resulting ionization potentials are in very good agreement with each other as well as with the very precise literature value from [23]. Notably, measurements could even be taken down to very low electric fields of $\sim$ 1V/cm, very close to the IP, without sizeable deviation from expectations. The accessible range of electric fields up to 200 V/cm ensured the determination of the IP with a relative precision of about $3 \cdot 10^{-6}$. In this way the application of the FI-LIST at a high-transmission mass separator like RISIKO or any on-line radioactive ion beam facility as e.g. ISOLDE at CERN, ISAC at TRIUMF, has been prepared and will facilitate IP determination also in complex spectra of elements available only in very limited quantities. This capability opens up new possibilities for studying this relevant atomic physics parameter in elements with challenging spectroscopic properties, e.g. in the range of the actinides, or investigating the trend of the IP along one isotopic chain far off stability. For elements that require specifically high temperatures for atomization, an issue that arises is the strongly increasing background from electron impact ionization at temperatures close to 2000 °C. To address this challenge, several adaptations can be considered for future refinements. In addition to simply increasing the potential at the electron repeller accordingly, which must be accompanied by a corresponding change of all potentials of the FI-LIST, temporal gating of these low voltage potentials can simply be implemented. Such a gating technique, synchronized to the laser pulses, ensures to focus on the desired laser ion signal while excluding or minimizing the far majority of background contributions [21]. The corresponding reduction of background counts improves the sensitivity of the measurements. Such tests are under way in preparation for IP measurements of actinide elements at RISIKO, i.e. in neptunium.

CRediT authorship contribution statement

Magdalena Kaja: Conceptualization, Formal analysis, Investigation, Methodology, Software, Visualization, Writing – original draft, Writing – review & editing. **Dominik Studer:** Conceptualization, Methodology, Software, Writing – review & editing. **Reinhard Heinke:** Conceptualization, Writing – review & editing. **Tom Kieck:** Conceptualization, Software, Writing – review & editing. **Klaus Wendt:** Conceptualization, Funding acquisition, Project administration, Supervision, Writing – review & editing.

Declaration of competing interest

The authors declare the following financial interests/personal relationships which may be considered as potential competing interests: Magdalena Kaja reports financial support was provided by European Unions Horizon 2020 Research and Innovation Programme under grant agreement project number 861198. Reinhard Heinke reports financial support was provided by the German Federal Ministry of Education and Research under the project 05P18UMCIA. Dominik Studer reports financial support was provided by the German Federal Ministry of Education and Research under the project 05P21UMFN3.

Data availability

Data will be made available on request.

Acknowledgments

We thank Mainz mechanical workshop team for constructing the FI-LIST parts. This work has received funding from the European Union's Horizon 2020 Research and Innovation Programme under grant agreement project number 861198 (LISA) Marie Sklodowska-Curie Innovative Training Network (ITN) as well as from the German Federal Ministry of Education and Research under the projects 05P18UMCIA and 05P21UMFN3.

References

[1] A. Kramida, Y. Ralchenko, J. Reader, NIST ASD Team, Nist atomic spectra database (ver. 5.10), 2022, [Online]. Available: https://physics.nist.gov/asd. (2 July 2023). National Institute of Standards and Technology, Gaithersburg, MD.

[2] C. Mattolat, T. Gottwald, S. Raeder, S. Rothe, F. Schwellnus, K. Wendt, P. Thörle-Pospiech, N. Trautmann, Determination of the first ionization potential of technetium, Phys. Rev. A 81 (5) (2010) 547, http://dx.doi.org/10.1103/PhysRevA.81.052513.

[3] S. Raeder, H. Heggen, A. Teigelhöfer, J. Lassen, Determination of the first ionization energy of polonium by resonance ionization spectroscopy - part I: Measurement of even-parity rydberg states at TRIUMF-ISAC, Spectrochim. Acta B 151 (2019) 65–71, http://dx.doi.org/10.1016/j.sab.2018.08.005.

[4] D.A. Fink, K. Blaum, V.N. Fedosseev, B.A. Marsh, R.E. Rossel, S. Rothe, Determination of the first ionization energy of polonium by resonance ionization spectroscopy – part II: Measurement of odd-parity rydberg states at CERN–ISOLDE, Spectrochim. Acta B 151 (2019) 72–82, http://dx.doi.org/10.1016/j.sab.2018.08.004.

[5] S. Rothe, A.N. Andreyev, S. Antalic, A. Borschevsky, L. Capponi, T.E. Cocolios, H. de Witte, E. Eliav, D.V. Fedorov, V.N. Fedosseev, D.A. Fink, S. Fritzsche, L. Ghys, M. Huyse, N. Imai, U. Kaldor, Y. Kudryavtsev, U. Köster, J.F.W. Lane, J. Lassen, V. Liberati, K.M. Lynch, B.A. Marsh, K. Nishio, D. Pauwels, V. Pershina, L. Popescu, T.J. Procter, D. Radulov, S. Raeder, M.M. Rajabali, E. Rapisarda, R.E. Rossel, K. Sandhu, M.D. Seliverstov, A.M. Sjödin, P. van den Bergh, P. van Duppen, M. Venhart, Y. Wakabayashi, K.D.A. Wendt, Measurement of the first ionization potential of astatine by laser ionization spectroscopy, Nat. Commun. 4 (2013) 1835, http://dx.doi.org/10.1038/ncomms2819.

[6] J. Roßnagel, S. Raeder, A. Hakimi, R. Ferrer, N. Trautmann, K. Wendt, Determination of the first ionization potential of actinium, Phys. Rev. A 85 (1) (2012) 1478, http://dx.doi.org/10.1103/PhysRevA.85.012525.

[7] N. Kneip, F. Weber, M.A. Kaja, C.E. Düllmann, C. Mokry, S. Raeder, J. Runke, D. Studer, N. Trautmann, K. Wendt, Investigation of the atomic structure of curium and determination of its first ionization potential, Eur. Phys. J. D 76 (190) (2022) http://dx.doi.org/10.1140/epjd/s10053-022-00510-7.

[8] F. Weber, T.E. Albrecht-Schönzart, M. Block, P. Chhetri, C.E. Düllmann, J.G. Ezold, V. Gadelshin, A.N. Gaiser, F. Giacoppo, R. Heinke, T. Kieck, N. Kneip, M. Laatiaoui, C. Mokry, S. Nothhelfer, S. Raeder, J. Runke, F. Schneider, J.M. Sperling, D. Studer, P. Thörle-Pospiech, N. Trautmann, K. Wendt, Atomic-structure investigations of neutral einsteinium by laser resonance ionization, Phys. Rev. Res. 4 (2022) 043053, http://dx.doi.org/10.1103/PhysRevResearch.4.043053.

[9] P. Chhetri, D. Ackermann, H. Backe, M. Block, B. Cheal, C. Droese, C.E. Düllmann, J. Even, R. Ferrer, F. Giacoppo, S. Götz, F.P. Heßberger, M. Huyse, O. Kaleja, J. Khuyagbaatar, P. Kunz, M. Laatiaoui, F. Lautenschläger, W. Lauth, N. Lecesne, L. Lens, E. Minaya Ramirez, A.K. Mistry, S. Raeder, P. van Duppen, T. Walther, A. Yakushev, Z. Zhang, Precision measurement of the first ionization potential of nobelium, Phys. Rev. Lett. 120 (26) (2018) 263003, http://dx.doi.org/10.1103/PhysRevLett.120.263003.

[10] P. Naubereit, T. Gottwald, D. Studer, K. Wendt, Excited atomic energy levels in protactinium by resonance ionization spectroscopy, Phys. Rev. A 98 (2) (2018) 022505, http://dx.doi.org/10.1103/PhysRevA.98.022505.

[11] P. Naubereit, D. Studer, A.V. Viatkina, A. Buchleitner, B. Dietz, V.V. Flambaum, K. Wendt, Intrinsic quantum chaos and spectral fluctuations within the protactinium atom, Phys. Rev. A 98 (2) (2018) 022506, http://dx.doi.org/10.1103/PhysRevA.98.022506.

[12] S. Köhler, R. Deissenberger, K. Eberhardt, N. Erdmann, G. Herrmann, G. Huber, J.V. Kratz, M. Nunnemann, G. Passler, P.M. Rao, J. Riegel, N. Trautmann, K. Wendt, Determination of the first ionization potential of actinide elements by resonance ionization mass spectroscopy, Spectrochim. Acta B 52 (6) (1997) 717–726, http://dx.doi.org/10.1016/S0584-8547(96)01670-9.

[13] N. Erdmann, M. Nunnemann, K. Eberhardt, G. Herrmann, G. Huber, S. Köhler, J.V. Kratz, G. Passler, J.R. Peterson, N. Trautmann, A. Waldek, Determination of the first ionization potential of nine actinide elements by resonance ionization mass spectroscopy (RIMS), J. Alloys Compounds 271–273 (1998) 837–840, http://dx.doi.org/10.1016/S0925-8388(98)00229-1.

[14] D. Studer, S. Heinitz, R. Heinke, P. Naubereit, R. Dressler, C. Guerrero, U. Köster, D. Schumann, K. Wendt, Atomic transitions and the first ionization potential of promethium determined by laser spectroscopy, Phys. Rev. A 99 (2019) 062513, http://dx.doi.org/10.1103/PhysRevA.99.062513.

[15] K. Blaum, C. Geppert, H.-J. Kluge, M. Mukherjee, S. Schwarz, K. Wendt, A novel scheme for a highly selective laser ion source, Nucl. Instrum. Methods Phys. Res. B 204 (2003) 331–335, http://dx.doi.org/10.1016/S0168-583X(02)01942-0, 14th International Conference on Electromagnetic Isotope Separators and Techniques Related to their Applications, URL https://www.sciencedirect.com/science/article/pii/S0168583X02019420.

[16] K. Wendt, K. Blaum, K. Brück, C. Geppert, H.-J. Kluge, M. Mukherjee, G. Passler, S. Schwarz, S. Sirotzki, K. Wies, A highly selective laser ion source for bunched, low emittance beam release, Nuclear Phys. A 746 (2004) 47–53, http://dx.doi.org/10.1016/j.nuclphysa.2004.09.067, Proceedings of the Sixth International Conference on Radioactive Nuclear Beams (RNB6), URL https://www.sciencedirect.com/science/article/pii/S037594740400956X.

[17] F. Schwellnus, K. Blaum, C. Geppert, T. Gottwald, H.-J. Kluge, C. Mattolat, W. Nörtershäuser, K. Wies, K. Wendt, The laser ion source and trap (LIST) – a highly selective ion source, Nucl. Instrum. Methods Phys. Res. B 266 (19) (2008) 4383–4386, http://dx.doi.org/10.1016/j.nimb.2008.05.065, Proceedings of the XVth International Conference on Electromagnetic Isotope Separators and Techniques Related to their Applications, URL https://www.sciencedirect.com/science/article/pii/S0168583X08007404.

[18] D. Fink, S. Richter, K. Blaum, R. Catherall, B. Crepieux, V. Fedosseev, A. Gottberg, T. Kron, B. Marsh, C. Mattolat, S. Raeder, R. Rossel, S. Rothe, F. Schwellnus, M. Seliverstov, M. Sjödin, T. Stora, P. Suominen, K. Wendt, On-line implementation and first operation of the laser ion source and trap at ISOLDE/CERN, Nucl. Instrum. Methods Phys. Res. B 344 (2015) 83–95, http://dx.doi.org/10.1016/j.nimb.2014.12.007, URL https://www.sciencedirect.com/science/article/pii/S0168583X14010222.

[19] D.A. Fink, T.E. Cocolios, A.N. Andreyev, S. Antalic, A.E. Barzakh, B. Bastin, D.V. Fedorov, V.N. Fedosseev, K.T. Flanagan, L. Ghys, A. Gottberg, M. Huyse, N. Imai, T. Kron, N. Lecesne, K.M. Lynch, B.A. Marsh, D. Pauwels, E. Rapisarda, S.D. Richter, R.E. Rossel, S. Rothe, M.D. Seliverstov, A.M. Sjödin, C. Van Beveren, P. Van Duppen, K.D.A. Wendt, In-source laser spectroscopy with the laser ion source and trap: First direct study of the ground-state properties of ^{217,219}Po, Phys. Rev. X 5 (2015) 011018, http://dx.doi.org/10.1103/PhysRevX.5.011018, URL https://link.aps.org/doi/10.1103/PhysRevX.5.011018.

[20] R. Heinke, T. Kron, S. Raeder, T. Reich, P. Schönberg, M. Trümper, C. Weichhold, K. Wendt, High-resolution in-source laser spectroscopy in perpendicular geometry, Hyperfine Interact. 238 (6) (2017) http://dx.doi.org/10.1007/s10751-016-1386-2.

[21] R. Heinke, M. Au, C. Bernerd, K. Chrysalidis, T.E. Cocolios, V.N. Fedosseev, I. Hendriks, A.A. Jaradat, M. Kaja, T. Kieck, T. Kron, R. Mancheva, B.A. Marsh, S. Marzari, S. Raeder, S. Rothe, D. Studer, F. Weber, K. Wendt, First on-line application of the high-resolution spectroscopy laser ion source PI-LIST at ISOLDE, Nucl. Instrum. Methods Phys. Res. B 541 (2023) 8–12, http://dx.doi.org/10.1016/j.nimb.2023.04.057.

[22] T. Kieck, H. Dorrer, C.E. Düllmann, V. Gadelshin, F. Schneider, K. Wendt, Highly efficient isotope separation and ion implantation of 163ho for the ECHo project, Nucl. Instrum. Methods Phys. Res. A 945 (2019) 162602, http://dx.doi.org/10.1016/j.nima.2019.162602.

[23] H. Lehec, A. Zuliani, W. Maineult, E. Luc-Koenig, P. Pillet, P. Cheinet, F. Niyaz, T.F. Gallagher, Laser and microwave spectroscopy of even-parity rydberg states of neutral ytterbium and multichannel-quantum-defect-theory analysis, Phys. Rev. A 98 (2018) 062506, http://dx.doi.org/10.1103/PhysRevA.98.062506.

[24] D.A. Dahl, SIMION Version 8.1.1, computer program, Idaho National Engineering and Environmental Laboratory.

[25] S. Rothe, B.A. Marsh, C. Mattolat, V.N. Fedosseev, K. Wendt, A complementary laser system for ISOLDE RILIS, J. Phys. Conf. Series 312 (5) (2011) 052020, http://dx.doi.org/10.1088/1742-6596/312/5/052020.

[26] A. Teigelhöfer, P. Bricault, O. Chachkova, M. Gillner, J. Lassen, J.P. Lavoie, R. Li, J. Meißner, W. Neu, K.D.A. Wendt, Grating tuned ti:Sa laser for in-source spectroscopy of rydberg and autoionizing states, Hyperfine Interact. 196 (1–3) (2010) 161–168, http://dx.doi.org/10.1007/s10751-010-0171-x.

[27] R. Li, M. Mostamand, J. Romans, J. Lassen, Polarization-dependent laser resonance ionization of beryllium, Spectrochim. Acta B 174 (2020) 105998, http://dx.doi.org/10.1016/j.sab.2020.105998.

[28] V.V. Kazakov, V.G. Kazakov, V.S. Kovalev, O.I. Meshkov, A.S. Yatsenko, Electronic structure of atoms: atomic spectroscopy information system, Phys. Scr. 92 (10) (2017) 105002, URL http://stacks.iop.org/1402-4896/92/i=10/a=105002.

[29] M.G. Littman, M.M. Kash, D. Kleppner, Field-ionization processes in excited atoms, Phys. Rev. Lett. 41 (1978) 103–107, http://dx.doi.org/10.1103/PhysRevLett.41.103, URL https://link.aps.org/doi/10.1103/PhysRevLett.41.103.

[30] F. Merkt, A. Osterwalder, R. Seiler, R. Signorell, H. Palm, H. Schmutz, R. Gunzinger, High rydberg states of argon: Stark effect and field-ionization properties, J. Phys. B: At. Mol. Opt. Phys. 31 (8) (1998) 1705, http://dx.doi.org/10.1088/0953-4075/31/8/020.